

BLAŽ LIKOZAR, MATJAŽ KRAJNC<sup>\*)</sup>

University of Ljubljana, Faculty of Chemistry and Chemical Technology  
Chair of Polymer Engineering and Organic Chemical Technology  
Aškerčeva cesta 5, 1000 Ljubljana, Slovenia

## Modeling of the dynamic mechanical properties of the coagent reinforced raw hydrogenated poly(butadiene-*co*-acrylonitrile) (HNBR) and the morphology of coagent nanodispersions in HNBR matrix

**Summary** — Coagents are typically used for crosslinking of synthetic elastomers and are ordinarily used to achieve excellent properties of the crosslinked products. Dynamic mechanical properties of two different types of reinforcing coagents and not cured hydrogenated poly(butadiene-*co*-acrylonitrile) compounds were investigated and modeled. The function of zinc dimethacrylate (ZDMA) inverted with loading in the mixtures from filler-like (up to 13 phr) into plasticizer-like behavior (over 13 phr). Nevertheless, trimethylolpropane trimethacrylate (TMPTMA) as a reinforcing substrate exhibited a reinforcing effect during the glass transition and plateau region throughout the investigated loading range. Morphology evolved during processing changed in parallel with the results obtained from dynamical mechanical analysis (DMA) of the blends. Both in the case of ZDMA and TMPTMA micro- and nano-phases evolved during mixing. The volume fractions of the particles under 100 nm in ZDMA and TMPTMA blends ranged from 16 to 89 %. Dynamic mechanical properties were modeled using a continuous relaxation distribution function, Williams-Landel-Ferry (WLF) equation and the modified Guth-Gold equation. The measured dynamic mechanical properties of not cured compounded elastomers containing coagents/fillers are of a great importance in connection with processing operations, which could be designed with aid of the proposed model.

**Key words:** hydrogenated poly(butadiene-*co*-acrylonitrile), curing coagents, reinforcement, dynamic mechanical properties, modeling.

MODELOWANIE DYNAMICZNYCH WŁAŚCIWOŚCI MECHANICZNYCH SUROWEGO UWODORNIONEGO POLI(BUTADIEN-*co*-AKRYLONITRYLU) (HNBR) WZMACNIANEGO WSPÓŁREAGENTEM SIECIOWANIA I MORFOLOGIA NANODYSERSJI WSPÓŁREAGENTA W MATRYCY HNBR

**Streszczenie** — Wyjaśniono rolę współreagenta w procesie sieciowania elastomerów. Zbadano dynamiczne właściwości mechaniczne układów HNBR/współreagent sieciowania oraz zaproponowano model opisujący wpływ ilości i rodzaju tego drugiego składnika na oceniane właściwości. Zastosowano dwa różne współreagenty, mianowicie dimetakrylan cynku (ZDMA) i trimetakrylan trimetylopropanu (TMPTMA). W miarę wzrostu stężenia ZDMA w układzie zmienia się efekt jego działania: zamiast wzmacniania (kompozycje 2–4, por. tabela 1) następuje plastyfikowanie (kompozycje 5–8), natomiast TMPTMA działa wzmacniająco w całym zbadanym zakresie składu. Wyniki badań właściwości mechanicznych metodą dynamicznej analizy mechanicznej (DMA) wskazują na zmiany morfologii układów zawierających zarówno ZDMA, jak i TMPTMA (rys. 1, 5, 6). Udział objętościowy cząstek o średnicy <100 nm w mieszaninach zawierających każdy ze współreagentów zmienia się w przedziale 16–89 % (tabela 2, rys. 4, 7, 8, 9). Szczegółowo opisano także modelowanie dynamicznych właściwości mechanicznych badanych kompozycji z wykorzystaniem ciągłej funkcji rozkładu relaksacji, równania Williama-Landela-Ferra (WLF) oraz zmodyfikowanego równania Guthe-Golda. Uzyskane wyniki mają istotne znaczenie z punktu widzenia projektowania procesów przetwórczych. **Słowa kluczowe:** uwodorniony poli(butadien-*co*-akrylonitryl), współreagenty sieciowania, wzmacnianie, dynamiczne właściwości mechaniczne, modelowanie.

### COAGENTS — THEIR ROLES AND BASIC TYPES

A coagent, or more specifically a peroxide curing coagent, is a multi-functional terminally unsaturated highly reactive towards free radicals monomeric or oli-

gomeric system that when used in the peroxide curing system enhances cross-linking. This occurs, while addi-

<sup>\*)</sup> To whom correspondence should be sent: matjaz.krajnc@fkkk.uni-lj.si

tion/polymerization, which is the principal mechanism by which it reacts in an elastomer compound, runs [1–3], it has been confirmed by studies in which the loss of coagent unsaturation during peroxide curing was observed [2, 4]. The most common coagents in the elastomer industry today are esters of acrylic or methacrylic acid, although the other types are used as well [5, 6]. Coagents are used with peroxide to increase the efficiency of curing [2, 7–9]. Also, when coagents are used in sufficient quantities, they cause changes in properties in addition to those associated with crosslinking efficiency [10]. Since coagents are nowadays quite standard in elastomer compounds' formulations, the knowledge of the processing of compounds becomes essential, especially if the addition of coagents affects rheological behavior. Zinc dimethacrylate (ZDMA) and trimethylolpropane trimethacrylate (TMPTMA) represent ones of the most commonly applied coagents.

ZDMA loaded peroxide cured hydrogenated poly(butadiene-*co*-acrylonitrile) commonly known as hydrogenated nitrile-butadiene elastomer (HNBR) was found to show high tensile strength [11–14]. Since then, several studies have been published on the topic of the ZDMA's outstanding reinforcement of elastomers. Ikeda *et al.* [15, 16] studied and simulated the *in situ* copolymerization behavior of ZDMA in HNBR during peroxide crosslinking. Recently, Lu *et al.* [17, 18] investigated the morphology and mechanical properties of ZDMA reinforced HNBR. Although most of the literature concerns ZDMA reinforced HNBR, the blends of ZDMA with other elastomers such as acrylonitrile/butadiene [17–20], styrene/butadiene [17, 18], ethylene/propylene/diene [17, 18, 21], ethylene/propylene [17, 18] and  $\alpha$ -octene/ethylene elastomer [17, 18, 22] were examined as well.

Addition of TMPTMA during elastomer processing is used to improve miscibility of elastomer itself and between elastomer and the other component. The polyfunctional monomer, such as TMPTMA, may reduce interfacial tension and increase the adhesion force between the polymer phases allowing finer dispersion and more stable morphology [23]. These advantages explain the fact that TMPTMA is widely employed and studied in many diverse systems and fields of application. Among others its blends with polyethylene [23–25], polypropylene [23], poly(ethylene-*co*-vinylacetate) [24, 26], ethylene/propylene/diene elastomer [27], acrylonitrile/butadiene elastomer [28], poly(vinyl chloride) [2, 9, 29, 30] and natural rubber [31] were investigated recently. Beside its application with peroxide crosslinked polymers, its effect on structural modification is advantageous even in the case of electron beam curing [24, 26–29, 31, 32].

In this publication the results of our study of the dynamic mechanical properties of not vulcanized HNBR compounds loaded with various amounts of ZDMA or TMPTMA as reinforcing substrates in selected ranges of

temperatures and oscillation frequencies are presented. The dynamic mechanical properties of the compounds were then modeled taking into account the effect of shear on the material properties, its temperature dependence and the impact of a reinforcing coagent/filler. The Williams-Landel-Ferry (WLF) equation [33] was applied for description of the compounds' frequency-temperature behavior whereas the reinforcing effect was described employing the modified Guth-Gold equation [34]. The reinforcing or plasticizing effect of the coagent was correlated with the compound morphology.

## EXPERIMENTAL

### Materials

HNBR used in this study was Zetpol 2020L, produced by Zeon Chemicals, with a nominal density equal to 950 kg/m<sup>3</sup>, 36.2 mol % bound acrylonitrile, iodine value equal to 28 mg/100 mg (91 mol % saturation) and Mooney viscosity ( $ML_{1+4, 100}^{\circ C}$ ) equal to 57.5. The average molecular weights ( $\overline{M}_n = 7.72 \cdot 10^4$  g/mol and  $\overline{M}_w = 2.36 \cdot 10^5$  g/mol) were determined by gel permeation chromatography (GPC, using Waters 2690 Separations Module) instrument with a refractive index detector. Three Waters Styragel columns (300 × 4.6 mm) were used in series. The HNBR solutions were prepared in tetrahydrofuran (THF) as a carrier solvent at a rate of 0.2 ml/min. The  $\overline{M}_n$  and  $\overline{M}_w$  values were calculated from molecular weight *versus* retention time curve of polystyrene standards.

**Table 1. Formulations of elastomer compounds ( $\pm$  0.001 g)**

Compound	1	2–7	8–13
Ingredient	Weight, g	Weight, g	Weight, g
HNBR	50	50	50
ZDMA	—	0.791, 1.582, 3.165 6.331, 12.663, 25.326	—
TMPTMA	—	—	1.000, 2.000, 4.000 8.000, 16.000, 32.000

The coagents were zinc dimethacrylate (ZDMA) from Aldrich (99 wt. % pure), with molar mass 235.5 g/mol and density 1485 kg/m<sup>3</sup>, and trimethylolpropane trimethacrylate (TMPTMA) absorbed on Microcel E (calcium silicate) from Akrochem (75 wt. % active ingredient), with trade name AKROSORB<sup>TM</sup> 29126, molar mass equal to 338.3 g/mol and density 1370 kg/m<sup>3</sup>. Formulations of the elastomer compounds are presented in Table 1.

### Processing

All components of the formulations were stored at 5 °C. They were mixed into the elastomer using the

Brabender Plasti-Corder PLD-Type 651 W 50 C, measuring mixer capable of maximum torque of 100 Nm at 30 °C. Temperature rose during mixing due to friction but has never exceeded 110 °C. Moreover, measuring mixer was hermetically closed to prevent any loss of components due to evaporation. Mixing was performed for 15 minutes, whereas the coagents were added after 5 minutes.

### Measurements

Samples for field emission scanning electron microscopy (FE-SEM) were cut from the compounds. Approximately 2 mm thick samples were then exposed to carbon vapor for sufficiently long time to achieve approximately 15 nm layer deposition. Micrographs were taken using FE-SEM (Zeiss, SUPRA 35 VP) at 1–20 kV utilizing different magnifications and contrasted using the quadrant back scattering detector (QBSD). Images were processed with AnalySIS 5.0 (Soft Imaging System).

Dynamic mechanical properties were measured in the shear mode using a DMA861<sup>e</sup> instrument from Mettler Toledo. Disc shaped samples were cut with thickness 1 ÷ 3 mm and diameter 13 ÷ 15 mm. Probing measurements were performed for various samples with thickness 1 ÷ 4 mm and with diameter ranging between 10 and 15 mm (instrument's software input) to confirm that the sample geometry had no effect on measured properties. Linearity check was executed, so that the measurements were performed within the linear viscoelastic regime that is within 10 N force amplitude and 10 μm displacement amplitude. Dynamic experiments were performed at temp. from -50 to 100 °C with constant heating rate ranging between 1 and 5 K/min at constant frequencies in the range 0.01 ÷ 100 Hz. All experiments were performed in an inert atmosphere.

Differential scanning calorimetry (DSC) measurements were conducted using a DSC 821<sup>e</sup> instrument from Mettler Toledo in nitrogen atmosphere (50 ml/min). The samples were prepared by weighing 3–11 mg of the compounds in 40 μl aluminum crucibles without pins. The samples were first heated from 20 °C to 100 °C in order to erase samples' thermal history, then quenched to -50 °C and finally again heated to 100 °C, with constant heating and cooling rates of 10 K/min. Indium and zinc standards were applied for the temperature calibration and for the determination of the instrument time constant.

The volume fraction of occluded elastomer was calculated from the dibutylphthalate (DBP) absorption in cubic centimeters of DBP per 100 g of elastomer. HNBR samples were immersed into DBP, which was left to absorb into elastomer samples until absorption endpoint, when the weight of samples ceased to vary with time and the endpoint concentration was calculated.

### RESULTS AND DISCUSSION

Viscoelastic properties of neat HNBR (compound 1) and its compounds with coagent/filler (compounds 2–13) were modeled. Storage modulus ( $G'$ ) and loss modulus ( $G''$ ) were measured in the frequency range between  $10^{-2}$  and  $10^2$  Hz during constant temperature increase of 1 K/min. Temperature behavior of storage modulus at the oscillation frequency of 1 Hz for HNBR/ZDMA compounds (compounds 2–7) is presented in Fig. 1. The effect of ZDMA on  $G'$  at lower loadings (compounds 2–4) resembles those for the fillers such as carbon black or silica in HNBR compounds [35, 36], which may be seen in Fig. 1(a). ZDMA has little effect on  $G'$  in the initial plateau region, that is the glassy state. It may be seen that ZDMA does not essentially shift the glass transition itself, as  $G'$  starts to decrease at relatively comparable temperatures.

The rubbery plateau ( $G'$  level) after the glass transition is the higher the larger is the amount of coagent/filler in the compound. The rubbery plateau for the compounds with lower ZDMA contents, in which the coagent acts as a reinforcing agent (compounds 2–4), starts at relatively similar temperatures, that is

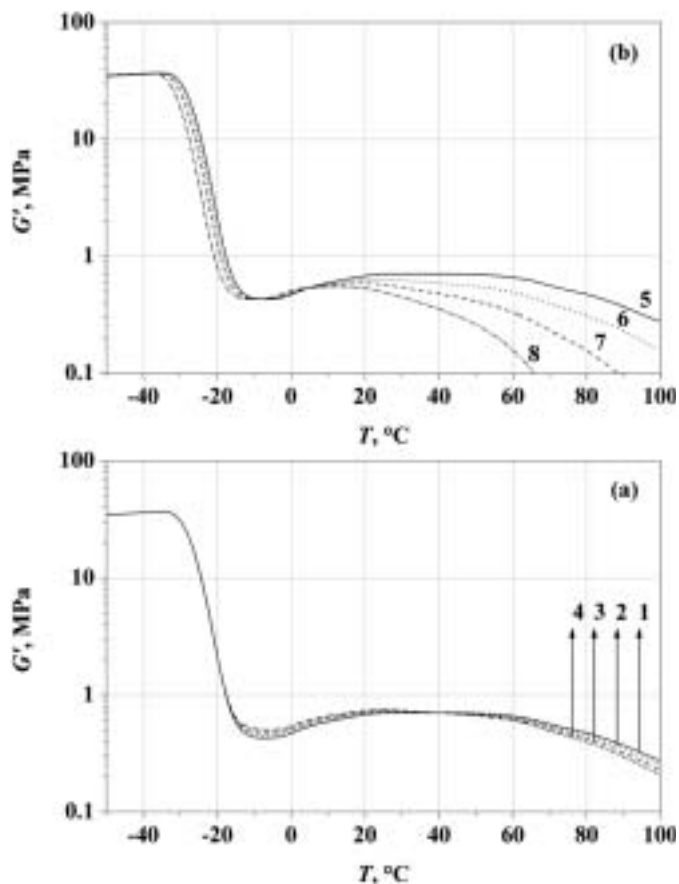


Fig. 1. Variation of storage modulus ( $G'$ ) with temperature (constant frequency 1 Hz and heating rate 1 K/min) for various amounts of ZDMA in the compound: (a) compounds 1–4, (b) compounds 5–8

around  $-7.5\text{ }^{\circ}\text{C}$ , what was determined as the temperature at which  $G'$  minima are reached. On the contrary, at higher ZDMA loadings, the latter acts as a plasticizer and shifts the rubbery plateau initiation towards lower temperatures, that is  $-8.3\text{ }^{\circ}\text{C}$ ,  $-9.1\text{ }^{\circ}\text{C}$  and  $-10.7\text{ }^{\circ}\text{C}$  for compounds 5, 6 and 7, respectively. The determination of the rubbery plateau termination is not so straightforward. As an unorthodox plateau behavior is encountered, one may only partially presume that the plateau termination may be correlated with the modulus decrease, after its maxima have been reached. This occurs at temperatures around  $24.5\text{ }^{\circ}\text{C}$  for the compounds 2–4 in comparison to neat elastomer (compound 1), which exhibits modulus decrease commencement (flow) at  $42.9\text{ }^{\circ}\text{C}$ . On the other hand, moduli of compounds 5, 6 and 7 begin to decrease at  $23.7\text{ }^{\circ}\text{C}$ ,  $18.1\text{ }^{\circ}\text{C}$  and  $11.3\text{ }^{\circ}\text{C}$ , respectively. Ordinarily, a raw elastomer would form a normal rubbery plateau after the glass transition; however, in this case a modulus build-up and consequential decrease are observed. This can be ascribed to the fact that HNBR occluded within the void of the aggregates of coagent/filler is not free to fully participate in the microscopic deformation of a compound [37, 38]. This immobilized elastomer may be identified with bound elastomer [39, 40], since it forms a complicated interlinked system with coagent/filler and is therefore not free.  $G'$  then increases from the rubbery plateau, but the more gradually the greater the amount of ZDMA. This happens when the structure ordering through the secondary bonds *i.e.* dipole-dipole interactions, is hindered, as the coagent/filler particles are percolated by HNBR network and the dipole-dipole interactions around these particles are not possible (Fig. 2) [41].

The elastomer occluded within the voids of primary coagent/filler aggregates [37, 38] as well as the portion of elastomer adsorbed or otherwise immobilized, is not

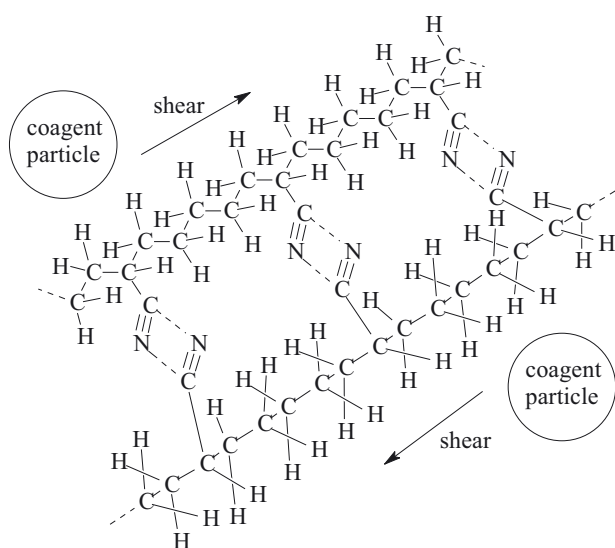


Fig. 2. Secondary bonding of HNBR chains and the hindrance due to the adsorption of chains (that is of polar groups, predominantly  $-\text{CN}$ ) onto ZDMA or TMPTMA particles

free to fully participate in the microscopic deformation of a coagent/filler and elastomer compound. Since the secondary bonds, *i.e.* dipole-dipole interactions, are principally determined by the frequency of acrylonitrile groups' encounters [41], the fraction of occluded elastomer is less likely to form secondary bonds. The reactivity ratios of the copolymerization of butadiene and acrylonitrile suggest that a reasonably alternating copolymer and a high concentration of acrylonitrile-butadiene dyads is obtained [42, 43]. Based on this fact, the molecular modeling on the model polymer chains, which consisted of 20 randomly distributed acrylonitrile and butadiene units in a chain, was performed. The chains were initially set apart and retained motionless in the glassy state. Afterwards, the geometry optimization was performed at the standard conditions using Polak-Ribiere (conjugate gradient) algorithm [44] with root-mean-square (RMS) gradient equal to  $0.0418\text{ kJ}/(\text{nm} \cdot \text{mol})$  as a terminal condition. The semi-empirical Parameterized Model number 3 (PM3) method of calculation, using unrestricted Hartree-Fock spin pairing and self-consistent field controls of 0.001 convergence limit and 1000 iterations limit, was applied. As the optimization terminated, the molecules shifted closer together and the secondary bonds among HNBR chains were formed as a result of the strong dipole-dipole interactions between the nitrile groups. There were several variations to the emerging bonds, but only a few kinds were frequently encountered upon their examination. These dipole-dipole interactions responsible for secondary bonding are presented in Fig. 3. It may be seen, that the distance between HNBR chains is maximal in the case of isolated dipole-dipole interactions [Fig. 3(a)], for the vicinal dipole-dipole interactions [Fig. 3(b)] it is smaller ( $0.472\text{ nm}$ ) and then it approaches the value  $0.494\text{ nm}$ , which is reached when at least two carbon atoms in the HNBR chain separate the dipole-dipole interactions [Fig. 3(d)]. This kind of bonding is also reported to be responsible for the structure ordering exhibited upon HNBR elongation [45]. In our case, however, the chains before the glass transition remain trapped in a state with little relative mobility, so the effect of bonding is not clearly exhibited. As the glass transition occurs, the chains gain some mobility and on one hand tend to orient upon shear and on the other they are more likely to form the secondary bonds, when individual nitrile groups' encounters become more frequent. In all cases presented in Fig. 1 these dipole-dipole interactions tend to build up until the temperature, when the formation of the secondary bonds upon shear is equilibrated by their dissociation due to the arising molecular motions, caused by elevated temperature. At the temperature of the equilibration the  $G'$  maximum is reached, after which HNBR gradually enters flow. This occurs at lower temperatures for ZDMA reinforced compounds, as a portion of elastomer is occluded and cannot take part in the secondary bonding and thus fewer overall dipole-dipole interac-

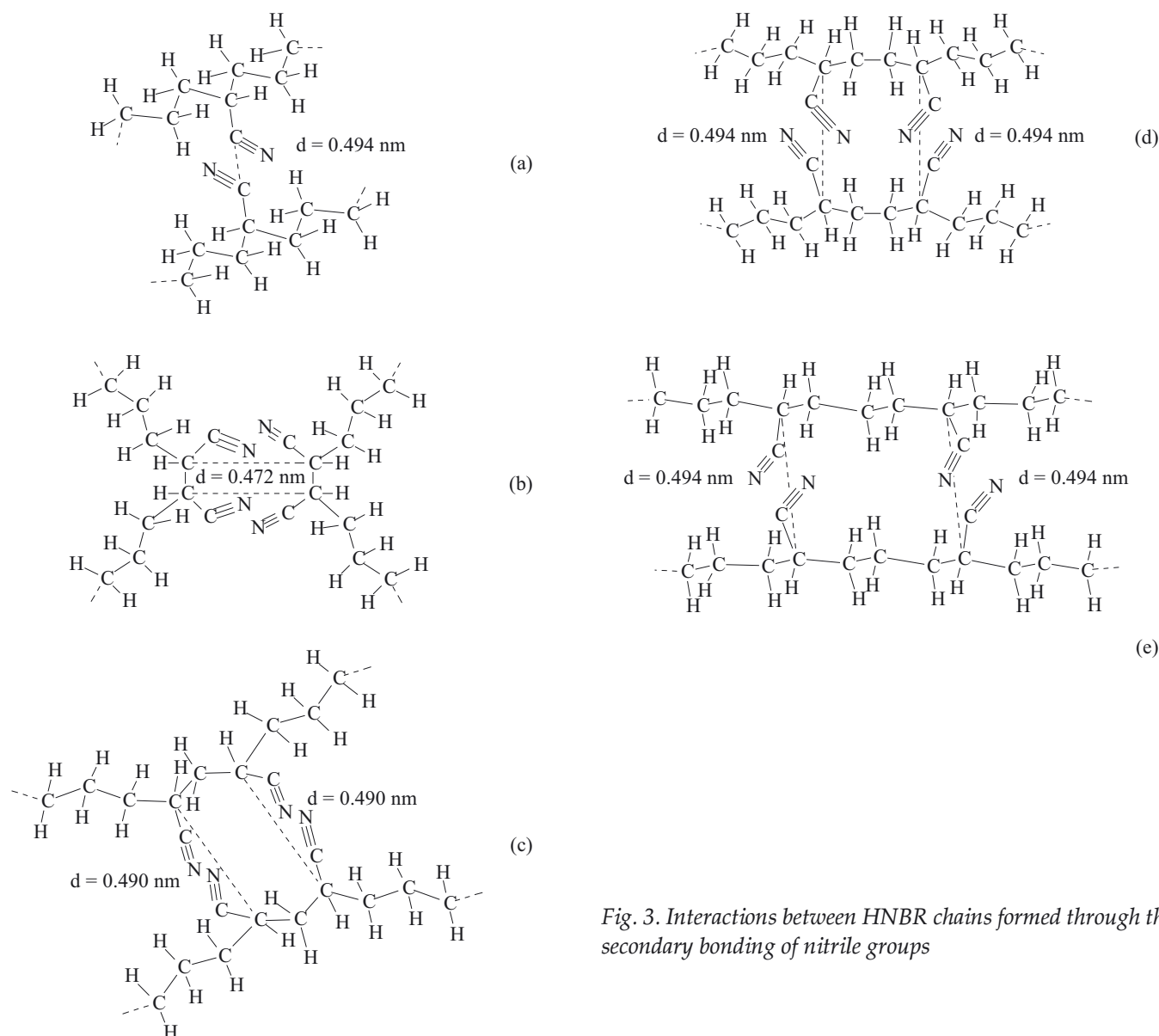


Fig. 3. Interactions between HNBR chains formed through the secondary bonding of nitrile groups

tions result in a lower modulus increase after the glass transition and even lower  $G'$  in the flow region. A decrease in flow behavior would normally be expected upon the introduction of a filler, but secondary bonding determine the commencement of flow behavior, thus inverting the filler action to inhibition as far as the mentioned ordering is concerned and resulting in the opposite trend in the flow initiation behavior.

At higher loadings, though, ZDMA exhibits a plasticizer-like behavior, which may be concluded from the temperature dependence of  $G'$  presented in Fig. 1(b). The glass transition shifts toward lower temperatures as the concentration of ZDMA in the compound is increased. Correspondingly,  $G'$  starts to decrease at lower temperatures. The apparent  $G'$  rise after the rubbery plateau observed for the compound 1 diminishes with increasing ZDMA content. This may be explained either by dilution of HNBR phase, which forms the secondary bonds responsible for the modulus increase, or by the slipping on HNBR/ZDMA interface. Furthermore, the evolution of more significantly expressed and broadly distributed

micro-phase fraction (see Fig. 7), at higher loadings of ZDMA (compounds 5—7) probably causes the inversion of reinforcing into softening behavior. This plasticizer-like behavior of HNBR/ZDMA compounds at higher loadings has been reported by Ikeda *et al.* [15]. On the contrary to the inversion of ZDMA functionality, TMPTMA exhibited reinforcing behavior throughout the whole studied range of its concentration in HNBR compound. Consequently, modeling of the reinforcing effect was limited for the compounds 2—4 and 8—13.

The frequency-temperature dependence of the moduli may be expressed by the equations (1) and (2) [46]:

$$\frac{G'(\omega, T)}{\rho(T)T} = \frac{G'(\omega a_T, T_R)}{\rho(T_R)T_R} \quad (1)$$

$$\frac{G''(\omega, T)}{\rho(T)T} = \frac{G''(\omega a_T, T_R)}{\rho(T_R)T_R} \quad (2)$$

where:  $\omega$  — frequency (rad/s),  $\rho$  — elastomer density,  $a_T$  — shift factor,  $T_R$  — reference temperature.

Therefore, in order to successfully model the frequency-temperature dependent moduli of the material a suitable expression for  $a_T$  had to be chosen and  $G'$  and  $G''$  at  $T_R$  had to be described. The dependence of elastomer density on temperature was obtained from our previous work [41] and applied for all compounds as it was observed that the incorporation of the coagent/filler did not noticeably affect the compound density (within the experimental error of density determination, which was approximately 5 %).

The most well known relationship between the shift factors and temperature, still most commonly used for numerous polymers [47], the WLF equation [33], was applied:

$$\lg a_T = \frac{-C_1(T-T_R)}{C_2+T-T_R} \quad (3)$$

The material constants  $C_1$  and  $C_2$  vary from polymer to polymer and may be linked to the Doolittle equation constants [48]. The dynamic mechanical properties of neat HNBR (compound 1) at  $T_R$  were described using the distribution functions [49]:

$$G'(\omega, T_R) = \int_{\ln \tau = -\infty}^{\ln \tau = \infty} H(\tau) \frac{\omega^2 \tau^2}{1 + \omega^2 \tau^2} d \ln \tau \quad (4)$$

$$G''(\omega, T_R) = \int_{\ln \tau = -\infty}^{\ln \tau = \infty} H(\tau) \frac{\omega \tau}{1 + \omega^2 \tau^2} d \ln \tau \quad (5)$$

where:  $H(\tau)$  — continuous distribution function at the specific relaxation time,  $\tau$ .

Since the objective of the modeling was not the estimation of the true continuous relaxation spectrum but rather the determination of the dynamic mechanical behavior of coagent/filler compounds in comparison to neat HNBR, an arbitrary distribution function was chosen for  $H(\tau)$ . The stress relaxation modulus for relatively straightforward relaxation processes may be thought to arise from a distribution of relaxation times that is composed of "a box and a wedge". This composite, originally suggested by Tobolsky [50] for poly(iso-butylene), was generalized as:

$$H(\tau) = \begin{cases} M/\tau^n, & \tau_1 < \tau < \tau_2 \\ E_0, & \tau_2 < \tau < \tau_m \end{cases} \quad (6)$$

The distribution described in equation (6) introduces variable parameters  $M$ ,  $n$  and  $E_0$  accompanied by integration interval endpoints  $\tau_1$ ,  $\tau_2$  and  $\tau_m$ . While the frequency-temperature behavior of neat HNBR (compound 1) may be described using equations (1)–(6), the effects of reinforcing coagents on dynamic mechanical properties still remains unaccounted. Thavamani and Bhowmick [35] showed that the modified Guth-Gold equation [equation (7)] [34] in the rubbery plateau for the various HNBR compounds rather well describes the relation between  $G'$  of the neat and the reinforced compounds using temperature independent effectiveness factor ( $Ef_R$ )

[34, 51] equal to 0.5 for the immobilized occluded elastomer.

$$G'^{RC} = (1 + 2.5 \cdot V + 14.1 \cdot V^2) \cdot G'_R \quad (7)$$

where: indexes  $R$  and  $RC$  — indicate rubbery region and reinforcing coagent, respectively,  $V$  — effective volume fraction of reinforcing coagent determined as.

$$V = Ef_R(\phi + \phi') \quad (8)$$

where:  $\phi$  — volume fraction of reinforcing coagent,  $\phi'$  — volume fraction of reinforcing coagent and immobilized elastomer combined.

The volume fraction of occluded elastomer ( $\phi' - \phi$ ) was calculated from dibutylphthalate (DBP) absorption [35, 37] (swelling of compounds without any solubility), while the effective volume fraction of reinforcing coagent ( $V$ ) was obtained by solving the quadratic equation, placed in equation (7). The effective volume fraction of reinforcing coagent ( $V$ ) has been found to be equal to the actual volume fraction ( $\phi$ ) plus a fraction of the occluded volume of elastomer (taken as equal to the volume of DBP in the aggregates at the DBP absorption endpoint) [34]. This may be expressed as:

$$V = Ef_R\phi\{1 + (1 + 0.02139[DBP]_{EP})/1.46\} \quad (9)$$

where:  $[DBP]_{EP}$  — amount of DBP ( $\text{cm}^3/100 \text{ g}$ ) at DBP absorption endpoint ( $136 \text{ cm}^3/100 \text{ g}$  for raw HNBR).

Dependence of the effective volume fraction of reinforcing coagent on the sum of the volume fraction of reinforcing coagent and the volume fraction of reinforcing coagent and immobilized elastomer combined should therefore be linear. Fig. 4 illustrates that the obtained overall plateau  $Ef_R$  is quite similar to the value proposed by Medalia [34, 51] and applied for HNBR by Thavamani and Bhowmick [35].

The model consisting of equations (1)–(8) was fitted to the experimental  $G'$  for the compounds 1–4 and

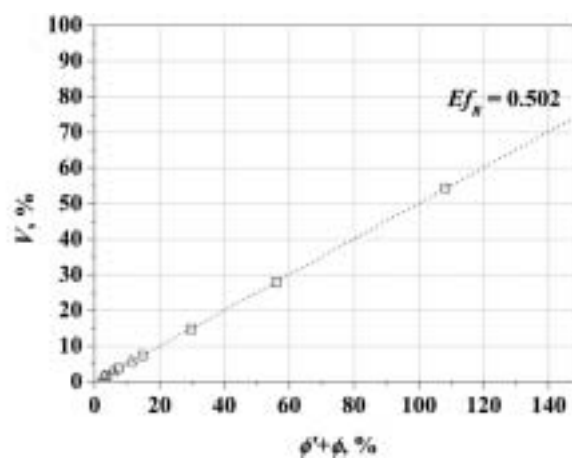


Fig. 4. Dependence of the effective volume fraction of reinforcing coagent ( $V$ ) on the sum of the volume fractions of reinforcing coagent ( $\phi$ ) and reinforcing coagent and immobilized elastomer combined ( $\phi + \phi'$ ) for ZDMA reinforced compounds ( $\Delta$ ) and TMPTMA reinforced compounds ( $\square$ )

8—13 and  $G''$  for the compound 1 using the Levenberg-Marquardt algorithm [52]. The glass transition temperature ( $T_g$ ) determined from the DSC thermogram for compound 1 ( $T_g = -27$  °C), which is the same as the one determined pycnometrically [41], was applied as the reference temperature. The continuous distribution function  $H(\tau)$  parameters may be firstly determined for neat elastomer alongside with the WLF equation parameters [53, 54], which is useful for lower coagent/filler loadings. In this work, however,  $H(\tau)$  and WLF equation parameters were determined simultaneously for compounds 1—4 and 8—13 to grant the best agreement throughout the entire range in which the coagent, that was either ZDMA or TMPTMA, acted as a reinforcing agent.

As the influence of reinforcing coagent is not the same throughout the entire temperature interval and frequency range, a temperature and frequency dependent  $Ef(\omega, T)$  was applied in the model. The temperature dependent effectiveness factor for the compounds 2—4 and 8—13 was obtained using the proposed equations:

$$G'(\omega, T)^{RC} = (1 + 2.5 \cdot V + 14.1 \cdot V^2) G'(\omega, T) \quad (10)$$

$$V = Ef(\omega, T)(\phi + \phi') \quad (11)$$

$$Ef(\omega, T) = \frac{G_G^{RC}}{G_G'} - 1 - \left( \frac{G_G^{RC}}{G_G'} - 1 - Ef_R \right) \left( 1 - \frac{G'(\omega, T) - G_R'}{G_G' - G_R'} \right) \quad (12)$$

where: *indexes G, R and RC indicate glassy region, rubbery region and reinforcing coagent, respectively.*

Equation (12) encompasses rather small influence of reinforcing coagent in the glassy region defined by the ratio  $G_G^{RC}/G_G' - 1$  and approaches the rubbery plateau value of  $Ef_R$  by following the behavior of neat elastomer's frequency and temperature dependent storage modulus.

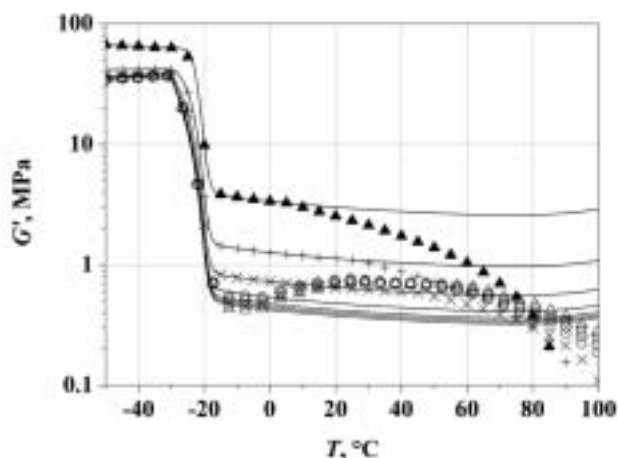


Fig. 5. Variation of  $G'$  with temperature (constant frequency 1 Hz and heating rate 1 K/min) for compounds 1 ( $\Delta$ ), 8 ( $\square$ ), 9 ( $\diamond$ ), 10 ( $\circ$ ), 11 ( $\times$ ), 12 ( $+$ ) and 13 ( $\blacktriangle$ ) and the model results (—)

Fig. 5 shows that the applied model consisting of equations (1)—(6) for the unfilled compound and of equations (1)—(12) for the compounds 2—4 and 8—13 relatively well coincides with the experimental results up to a certain temperature, when the secondary bonding starts to become more distinct. The effect of TMPTMA on the reinforcing substrate resembles the one of ZDMA at lower loadings [Fig. 1(a)]. In the case of TMPTMA effect on the reinforcing substrate, the reinforcing effect persists throughout the entire range of loadings examined, principally due to the nature of the substrate itself. Moreover, the impact of the hindered secondary bonding becomes even more pronounced at higher loadings as the modulus increase after the rubbery plateau may no longer be observed for the compounds 10—13.

The continuous distribution function parameters at sufficiently long  $\tau_m$  were found to be 0.125 ( $n$ ), 3.89 MPa  $\cdot$  s<sup>0.125</sup> ( $M$ ) and 1.18  $\cdot$  10<sup>-2</sup> MPa ( $E_0$ ) with corresponding integration interval endpoints 4.35  $\cdot$  10<sup>-3</sup> s ( $\tau_1$ ) and 7.94 s ( $\tau_2$ ). The continuous distribution function parameters are relatively similar to the ones obtained from independent fitting of the model to the experimental data for neat HNBR [53], yet grant better overall agreement of the experimental and predicted values of  $G'$ . Furthermore, the minute deviation of the continuous distribution function parameters determined in this study from the ones determined for neat elastomer implies that the equations (7)—(12) are suitable for the description of reinforcing effect, observed for compounds 2—4 and 8—13.

ZDMA and TMPTMA powders were prepared so that the majority of particles (more than 90 %) had a relatively uniform maximal dimension between 1 and 2  $\mu$ m prior to compound preparation. The particles tended to be rather irregular, while some could be considered spherical, whereas the same authors observed rod-like ZDMA particles. ZDMA particle surface consisted of fiber-like structures, which were also observed by the same authors and were ascribed to ZDMA microcrystals. On the other hand, further enlargement of observed TMPTMA particles did not reveal any periodic pattern saved for certain degree of irregularity. Except for the latter the surface of TMPTMA particles appeared to be relatively smooth. An example of SEM images is presented in Fig. 6. Analysis of the images obtained from FE-SEM measurements at various magnifications and experimental conditions revealed that the compounds (compounds 2—13) were rather homogeneous and isotropic (in terms of multiple sampling of the compounds at different positions) considering the distribution of the coagent/filler particles.

The morphology of the compounds in terms of particle size distribution is presented in Fig. 7 and 8 for ZDMA and TMPTMA containing compounds, respectively. The morphology of HNBR/ZDMA and HNBR/TMPTMA compounds is diphasic in nature, with

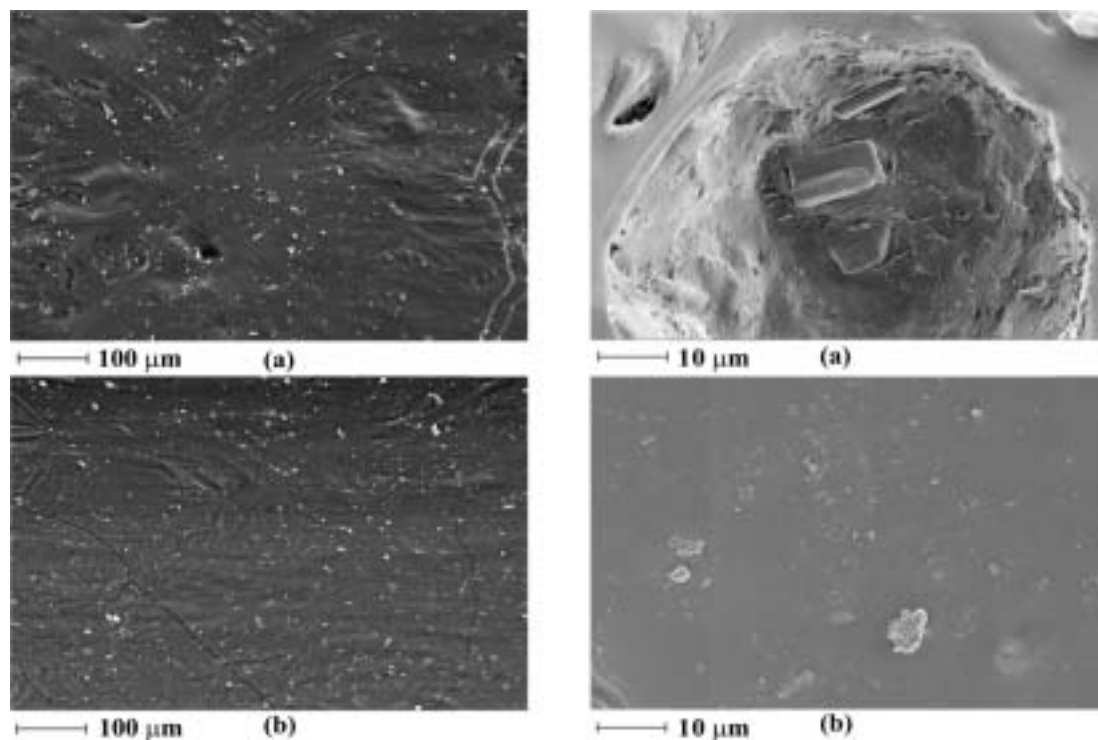


Fig. 6. Scanning electron micrographs of: (a) HNBR/ZDMA compound (compound 4) and (b) HNBR/TMPTMA compound (compound 10)

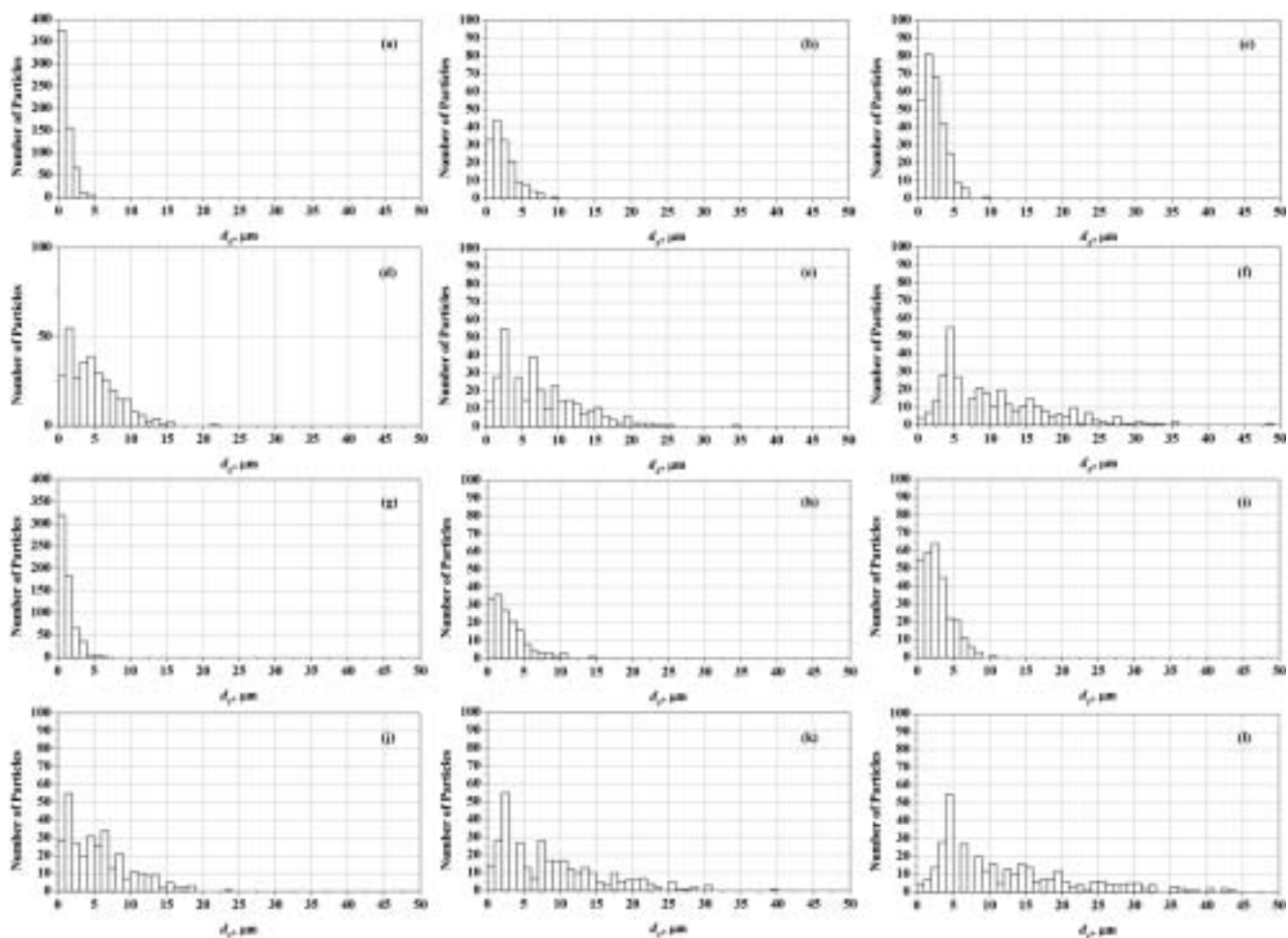


Fig. 7. Size distribution of particles larger than 100 nm in HNBR/ZDMA compounds: (a) compound 2, (b) compound 3, (c) compound 4, (d) compound 5, (e) compound 6 and (f) compound 7 ( $d_E$ ); (g) compound 2, (h) compound 3, (i) compound 4, (j) compound 5, (k) compound 6 and (l) compound 7 ( $d_F$ )

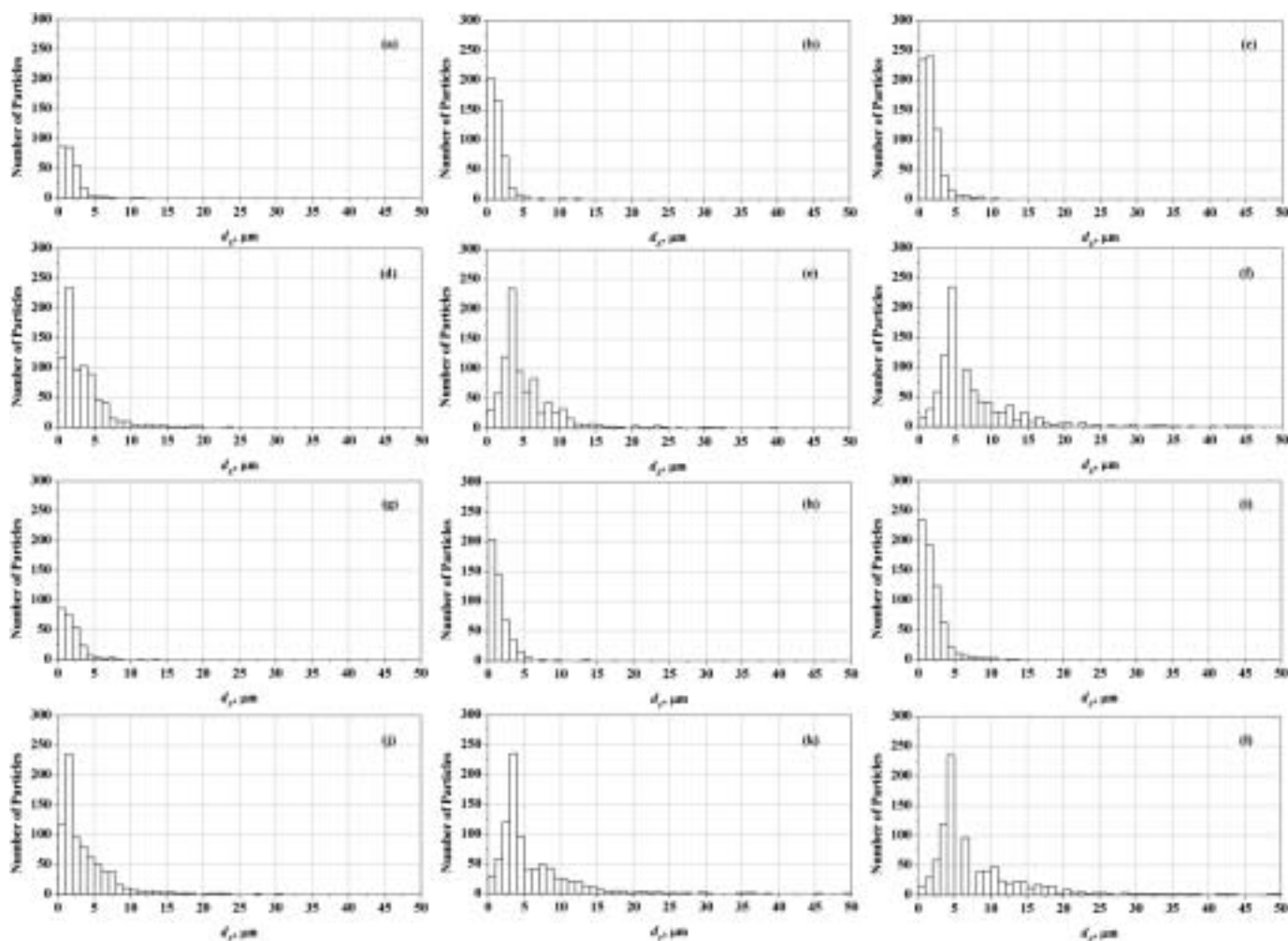


Fig. 8. Size distribution of particles larger than 100 nm in HNBR/TMPTMA compounds: (a) compound 8, (b) compound 9, (c) compound 10, (d) compound 11, (e) compound 12 ( $d_E$ ) and (f) compound 13, (g) compound 8, (h) compound 9, (i) compound 10, (j) compound 11, (k) compound 12 and (l) compound 13 ( $d_F$ )

ZDMA or TMPTMA particles distributed in HNBR matrix.

The morphology of the compounds 2–13 was examined statistically with arbitrarily chosen particle size threshold 100 nm (considering the resolution at the appropriate magnification to encompass statistically all particle sizes top-down). Several surfaces of the same compound were examined at different magnifications. The histograms in Fig. 7 indicate that at the lower concentration of ZDMA in the compound the greatest number of particles does not exceed micrometer size. At higher concentrations, however, two ZDMA phases become more distinct, since the greatest fraction of the micro-phase is between 1 and 2  $\mu\text{m}$  for compounds 3–5 and even shifts towards higher particle sizes for compound 6 (2–3  $\mu\text{m}$ ) and compound 7 (4–5  $\mu\text{m}$ ).

If the distributions of particles' sizes are compared regarding equivalent circular diameter ( $d_E$ ) [Fig. 7(a)–7(f)] and mean Feret diameter ( $d_F$ ) [Fig. 7(g)–7(l)], the conclusion may be made that the particles may be considered spherical, since the distributions are rela-

tively similar regardless of the characteristic dimension. Histograms in Fig. 8, though, indicate that in TMPTMA containing compounds the greatest number of particles is below micrometer size in compounds 8 and 9. Nevertheless, in the case of TMPTMA, the micro-phase evolution becomes visible between 1 and 2  $\mu\text{m}$  for compounds 10 and 11. The largest portion of particles has even greater  $d_E$  and  $d_F$  in compounds 12 and 13. The evolution of predominating micro-phase seems to occur in the case of TMPTMA at higher loadings than in the case of ZDMA. In the TMPTMA containing compounds, the co-agent particles also tend to form a spherical shape, which may be seen upon comparing the distributions of  $d_E$  and  $d_F$ . Another distinction between ZDMA and TMPTMA dispersions, which may be seen upon comparison of Fig. 7 and 8 is, that the distributions of ZDMA particles at higher loadings of ZDMA in the matrix become wider and more asymmetrical due to a portion of micro-phase particles tending towards larger  $d_E$ . The addition of crosslinking agent, such as dicumyl peroxide, does not seem to affect the distribution of the co-agent/filler in the elastomer matrix [53].

In view of the fact that the micrographs were subjected to the statistical treatment with the particle size threshold of 100 nm, the nano-phase volume fraction normalized to the total coagent volume fraction may be calculated according to the equation (13) taking into account the assumptions of relatively spherical particles, homogeneity and isotropy of the compounds:

$$\phi = 1 - \frac{\frac{\pi}{4} \sum_{i=1}^I d_{Ei}^2 \left( 1 + \frac{w_{HNBR} \rho_{Coagent}}{w_{Coagent} \rho_{HNBR}} \right)}{A} \quad (13)$$

where:  $\phi$  — nano-phase volume fraction,  $w$  — weight fraction,  $\rho$  — density,  $A$  — area of the micrograph subjected to statistical treatment.

**Table 2.** Fraction of particles under 100 nm for HNBR/ZDMA and HNBR/TMPTMA compounds (determined by processing of FE-SEM images)

Compound	Volume of particles under 100 nm per total coagent volume, vol. %	Volume of particles under 100 nm per total HNBR volume, vol. %
HNBR/ZDMA (compound 2)	78.8	0.80
HNBR/ZDMA (compound 3)	86.1	1.74
HNBR/ZDMA (compound 4)	89.0	3.60
HNBR/ZDMA (compound 5)	53.0	4.29
HNBR/ZDMA (compound 6)	31.3	5.07
HNBR/ZDMA (compound 7)	16.6	5.40
HNBR/TMPTMA (compound 8)	80.7	1.11
HNBR/TMPTMA (compound 9)	87.7	2.43
HNBR/TMPTMA (compound 10)	88.5	4.91
HNBR/TMPTMA (compound 11)	50.1	5.56
HNBR/TMPTMA (compound 12)	25.3	5.61
HNBR/TMPTMA (compound 13)	12.7	5.64

The nano-phase in the compound consists of fiber-like dispersion structures with maximal Feret diameters lower than 100 nm, which is likely related to the fiber-like structure at ZDMA surface [17]. The nano-phase fractions are presented in Table 2. Both in the ZDMA and TMPTMA containing compounds the fractions increase with the coagent concentration, yet it may be noted that even initial increase is not linear if the coagent loading is twofold or four times that of the one in the compound 2 or 8 for ZDMA or TMPTMA, respectively. After the fraction of nano-phase reaches its maximal values of 89.0 vol. % and 88.5 vol. % for ZDMA and TMPTMA, respectively, it starts to decrease. This implies that there is some boundary saturation of elastomer phase with the nano-phase after which the evolution of micro-phase becomes more explicit. In Table 2, this may be observed as the asymptotic increase in the nano-phase regarding its portion in comparison to the total HNBR volume. Overall,

the volume fraction of the nano-phase at lower loadings of coagent/filler is substantial either in ZDMA or TMPTMA containing compounds. During mechanical mixing a large number of micro-level particles were thus ground into smaller particles and even ultra-fine particles which sizes were nano-level, led to the reduction in dimension and amount of micro-level particles in HNBR [17]. However, aggregation proceeded simultaneously.

In view of the nano- and micro-phase evolution in either ZDMA or TMPTMA reinforced compounds the viscoelastic behavior may be examined once again. At lower loadings both coagents exhibited reinforcing effect, which can be ascribed to rather large portions of the coagent segregated in the form of nano-phase (Table 2). At higher loadings, though, the average ZDMA particle gains in size, resulting in lower fraction of rigid and reinforcing nano-phase on account of apparently matrix-softening micro-fraction. The impact of bonding among zinc and methacrylate ions thus becomes negligible in comparison to the softening ZDMA particles. This, however, does not occur in the case of TMPTMA, principally due to the filler-like behavior of the substrate (calcium silicate) itself.

Whether the amount of immobilized elastomer, calculated from dibutylphthalate absorption, should be considered? It may be concluded that for lower loadings of either ZDMA or TMPTMA it increases linearly with either nano- or micro-phase volume fraction (Fig. 9), following low nano-fraction and low micro-fraction

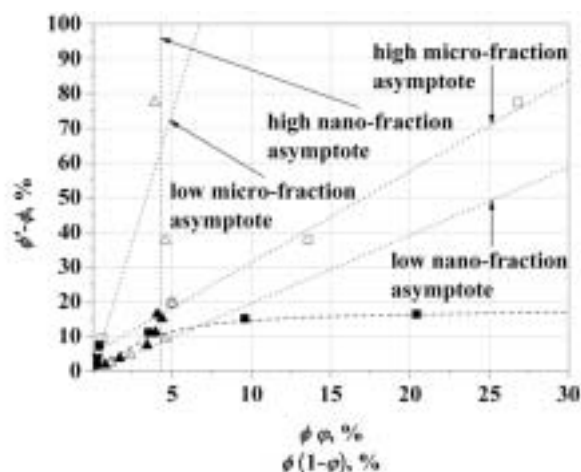


**Fig. 9.** Immobilized elastomer fraction ( $\phi' - \phi$ ) for the various fractions of ZDMA ( $\blacktriangle$ ) or TMPTMA ( $\triangle$ ) nano-phase ( $\phi$ ) and ZDMA ( $\blacksquare$ ) or TMPTMA ( $\square$ ) micro-phase [ $\phi(1 - \phi)$ ]

asymptotes. This suggests that the dispersions of coagent (either ZDMA or TMPTMA) in the elastomer matrices are similar. Moreover, regarding the dependence of the immobilized elastomer on both micro- and nano-phase fractions one may come to conclusion that the nano-phase mostly determines the amount of the immo-

bilized elastomer due to its wide distribution (Table 2) and consequentially relatively large specific elastomer/coagent interface surface, principally responsible for the immobilization of elastomer through adsorption of its molecules. At the higher loadings of both coagents, the behavior varies for ZDMA and TMPTMA. The one thing both coagents have in common at higher loadings is that the nano-phase ceases to predominately determine the amount of the immobilized elastomer, which increases, regardless of the unchanging concentration of the nano-phase following the high nano-fraction asymptote.

### CONCLUSIONS

Dynamic mechanical properties of ZDMA/HNBR and TMPTMA/HNBR compounds after mixing were investigated. ZDMA at lower loadings (up to 13 phr) in a compound as well as TMPTMA in the whole range of the loadings exhibited the reinforcement of HNBR matrix, whereas in the case of ZDMA the inversion of reinforcing (up to 13 phr) into a plasticizer-like behavior (over 13 phr) ensued upon increase in ZDMA loading in a compound. The dynamic mechanical properties of reinforced compounds were modeled combining a continuous distribution function, which was applied to describe the relaxation behavior of neat elastomer at the chosen reference temperature [parameters at sufficiently long  $\tau_m$  were found to be  $0.125 (n)$ ,  $3.89 \text{ MPa} \cdot \text{s}^{0.125} (M)$  and  $1.18 \cdot 10^{-2} \text{ MPa} (E_0)$  with corresponding integration interval endpoints  $4.35 \cdot 10^{-3} \text{ s} (\tau_1)$  and  $7.94 \text{ s} (\tau_2)$ ], using the WLF equation, which served for the description of the frequency-temperature superposition, and the modified Guth-Gold equation ( $E_{fR}$  was determined at 0.502, that is basically at its theoretical value of 0.5) taking into account the reinforcing effect of coagent/filler. The continuous distribution function and the WLF equation parameters were determined simultaneously for all the examined compounds, while the rubbery plateau effectiveness factor (the dependence of  $V$  on the sum of  $\phi$  and  $\phi'$  was linear throughout the reinforcing loading range of both ZDMA and TMPTMA) and the portion of immobilized elastomer (up to 78 vol. %) were determined from the plateau moduli and by utilization of the absorption studies, respectively. The model predictions agreed well with the experimental results up to a temperature over the rubbery plateau, when the cyano group secondary bonding occurred.

Both for ZDMA and TMPTMA at lower loadings in a compound the nano-phase fractions in the compounds prevailed and determined the amount of the immobilized elastomer, while at their higher loadings the micro-fraction became more distinct and proved to be predominant in determining the reinforcing characteristics of TMPTMA. On the other hand, the evolution of prevailing micro-fraction in ZDMA/HNBR compounds caused the softening of the matrix as the role of bonding

among zinc and methacrylate ions, decisive for reinforcement at lower loadings, decreased. This was observed as gradual reduction of the amount of the immobilized elastomer upon raising the ZDMA loading and more clear evolution of its micro-phase.

### REFERENCES

- [1] Ogunniyi D.: *Rubber Chem. Technol.* 2000, **73**, 74. [2] Yáñez-Flores I. G., Ibarra-Gómez R., Rodríguez-Fernández O. S., Gilbert M.: *Eur. Polym. J.* 2000, **36**, 2235. [3] Oh S. J., Koenig J. L.: *Prog. Rubber Plast. Technol.* 1999, **15**, 95. [4] Murgic Z. H., Jelencic J., Murgic L.: *Polym. Eng. Sci.* 1998, **38**, 689. [5] Drake R. E., Holliday J. J., Costello M. S.: *Rubber World* 1995, **213**, 22. [6] Tuccio A.: *Rubber World* 1994, **209**, 34. [7] Yu Q., Zhou S.: *J. Polym. Sci., Pol. Chem.* 1998, **36**, 851. [8] Bucsi A., Szocs F.: *Macromol. Chem. Phys.* 2000, **201**, 435. [9] García-Quesada J. C., Gilbert M.: *J. Appl. Polym. Sci.* 2000, **77**, 2657. [10] Class J.: *Rubber World* 1999, **220**, 35.
- [11] *Pat. Jap* 01 306 440 (1988). [12] *Pat. Jap.* 01 306 441 (1988). [13] *Pat. Jap.* 01 306 443 (1988). [14] Inoue T.: *Prog. Polym. Sci.* 1995, **20**, 119. [15] Ikeda T., Yamada B., Tsuji M., Sakurai S.: *Polym. Int.* 1999, **48**, 446. [16] Ikeda T., Yamada B.: *Polym. Int.* 1999, **48**, 367. [17] Lu Y., Liu L., Yang C., Tian M., Zhang L.: *Eur. Polym. J.* 2005, **41**, 577. [18] Lu Y., Liu L., Tian M., Geng H., Zhang L.: *Eur. Polym. J.* 2005, **41**, 589. [19] Samui A. B., Dalvi V. G., Chandrasekhar L., Patri M., Chakraborty B. C.: *J. Appl. Polym. Sci.* 2006, **99**, 2542. [20] Yuan X., Peng Z., Zhang Y., Zhang Y.: *J. Appl. Polym. Sci.* 2000, **77**, 2740.
- [21] Peng Z., Liang X., Zhang Y., Zhang Y.: *J. Appl. Polym. Sci.* 2002, **84**, 1339. [22] Lu Y., Liu L., Shen D., Yang C., Zhang L.: *Polym. Int.* 2004, **53**, 802. [23] Ali Z. I., Youssef H. A., Said H. M., Saleh H. H.: *Thermochim. Acta* 2005, **438**, 70. [24] Dadbin S., Frounchi M., Sabet M.: *Polym. Int.* 2005, **54**, 686. [25] Tai H. J.: *Polym. Eng. Sci.* 2001, **41**, 95. [26] Datta S. K., Bhowmick A. K., Chaki T. K., Majali A. B., Deshpande R. S.: *Polymer* 1996, **37**, 45. [27] Chowdhury R., Banerji M. S.: *J. Appl. Polym. Sci.* 2005, **97**, 968. [28] Yasin T., Ahmed S., Yoshii F., Makuuchi K.: *React. Func. Polym.* 2003, **57**, 113. [29] Youssef H. A., Ali Z. I., Zahran A. H.: *Polym. Deg. Stab.* 2001, **74**, 213. [30] Saethre B., Gilbert M.: *Polymer* 1996, **37**, 3379.
- [31] Jayasuriya M. M., Makuuchi K., Yoshi F.: *Eur. Polym. J.* 2001, **37**, 93. [32] Banik I., Dutta S. K., Chaki T. K., Bhowmick A. K.: *Polymer* 1999, **40**, 447. [33] Williams M. L., Landel R. F., Ferry J. D.: *J. Amer. Chem. Soc.* 1955, **77**, 3701. [34] Medalia A. I.: *Rubber Chem. Technol.* 1973, **46**, 877. [35] Thavamani P., Bhowmick A. K.: *J. Mater. Sci.* 1992, **27**, 3243. [36] Manoj N. R., De S. K., De P. P.: *Rubber Chem. Technol.* 1993, **66**, 550. [37] Medalia A. I.: *J. Colloid Interface Sci.* 1970, **32**, 115. [38] Kraus G.: *J. Polym. Sci.* 1970, **8**, 601. [39] Gessler A. M.: *Rubber Age* 1969, **101**, 54. [40] Medalia A. I.: *Rubber Chem. Technol.* 1974, **47**, 411.
- [41] Likozar B., Krajnc M.: *E-Polymers* 2007, **131**, 1. [42] Severe G., White J. L.: *J. Appl. Polym. Sci.* 2000, **78**,

1521. [43] Severe G., White J. L.: *Kautsch. Gummi Kunstst.* 2002, **55**, 144. [44] Hestenes M. R., Stiefel E.: *J. Res. Natl. Bur. Stand.* 1952, **49**, 409. [45] Bieliński D. M., Ślusarski L., Włochowicz A., Ślusarczyk C.: *J. Appl. Polym. Sci.* 1998, **67**, 501. [46] Plazek D. J.: *J. Phys. Chem.* 1965, **69**, 3480. [47] Ferry J. D.: "Viscoelastic Properties of Polymers", John Wiley & Sons, Inc., New York 1980, p. 280. [48] Doolittle A. K., Doolittle D. B.: *J. Appl. Phys.* 1957, **28**, 901. [49] Shaw M. T., MacKnight W. J.: "Introduction to Polymer

Viscoelasticity", John Wiley & Sons, Inc., Hoboken 2005, p. 107. [50] Tobolsky A. V.: "Properties and Structure of Polymers", Wiley, New York 1960, p.128, p.151.

[51] Medalia A. I.: *Rubber Chem. Technol.* 1972, **45**, 1172. [52] Marquardt D.: *SIAM J. Appl. Math.* 1963, **11**, 431. [53] Likozar B., Krajnc M.: *J. Appl. Polym. Sci.* 2008, **110**, 183. [54] Likozar B., Šebenik U., Krajnc M.: *Polym. Eng. Sci.* 2007, **47**, 2085.

Received 14 III 2008.

INSTYTUT INŻYNIERII MATERIAŁÓW POLIMEROWYCH I BARWNIKÓW W TORUNIU  
ODDZIAŁ ZAMIEJSCOWY FARB I TWORZYW W GLIWICACH



zaprasza do zaprezentowania swoich osiągnięć  
na VIII Międzynarodowej Konferencji



## ADVANCES IN PLASTICS TECHNOLOGY (POSTĘPY W TECHNOLOGII TWORZYW POLIMEROWYCH)

która odbędzie się w dniach 3–5 listopada 2009 r. na terenie Międzynarodowych Targów Katowickich, Katowice, ul. Bytkowska 1b.

**Przewodniczący Komitetu Naukowego** — prof. dr hab. inż. Marian Żenkiewicz, Instytut Inżynierii Materiałów Polimerowych i Barwników w Toruniu.

**Przewodnicząca Komitetu Organizacyjnego** — mgr inż. Anna Pająk, Instytut Inżynierii Materiałów Polimerowych i Barwników w Toruniu, Oddział Zamiejscowy Farb i Tworzyw w Gliwicach.

**Tematyka Konferencji obejmuje:**

- Nowości w zakresie bazy surowcowej dla tworzyw (polimery, pigmenty, napelniacze)
- Nowe generacje środków pomocniczych i modyfikatorów
- Osiągnięcia w zakresie przetwórstwa tworzyw i ich stosowania
- Nowoczesne rozwiązania dotyczące maszyn i oprzyrządowania w przetwórstwie tworzyw
- Ochronę środowiska naturalnego, recykling, regulacje prawne
- Zagadnienia badawcze i rozwojowe oraz kontrolno-pomiarowe
- Badania rynku

Językiem konferencji będzie język angielski z symultanicznym tłumaczeniem na język polski.

Wszystkie materiały, tj.: skrót referatu lub plakatu (do 120 słów), biografia autora (do 50 słów), pełny tekst referatu lub plakatu (do 10 stron formatu A-4), powinny być dostarczone w języku angielskim. Czas prezentacji referatu wynosi ok. 30 minut (wraz z dyskusją).

**Będzie możliwość promocji firmy w formie wkładki reklamowej, plakatu lub stanowiska promocyjnego w czasie trwania konferencji.**

Koszt udziału w konferencji dla osoby wygłaszającej referat lub prezentującej poster wynosi 200 euro (brutto).

Tytuł referatu lub plakatu wraz z jego skrótem oraz biografia osoby prezentującej powinny być dostarczone w terminie do **15 czerwca 2009 r.** na adres: Instytut Inżynierii Materiałów Polimerowych i Barwników, Oddział Zamiejscowy Farb i Tworzyw w Gliwicach, Komitet Organizacyjny Konferencji APT '09, ul. Chorzowska 50A, 44-100 Gliwice.

Informacje o konferencji — mgr inż. Anna Pająk, tel. +48 (32) 231 9043; fax: +48 (32) 231 2674; e-mail: a.pajak@impib.pl, www.impib.pl